Supporting Information

Integrated carbon capture and CO production from bicarbonates through bipolar membrane electrolysis

Hakhyeon Song[1,2,4], Carlos A. Fernández[1,4], Hyeonuk Choi[3,4], Po-Wei, Huang[2], Jihun Oh[3,*], and Marta C. Hatzell[1,2,*]

*Corresponding Author

Jihun Oh: jihun.oh@kaist.ac.kr

Marta C. Hatzell: marta.hatzell@me.gatech.edu

[1] George W. Woodruff School of Mechanical Engineering, Georgia Institute of Technology, Atlanta, GA 30332, United States

[2] School of Chemical and Biomolecular Engineering, Georgia Institute of Technology, Atlanta, GA 30332, United States

[3] Department of Materials Science and Engineering, Korea Advanced Institute of Science and Technology (KAIST), 291 Daehak-ro, Yuseong-gu, Daejeon 34141, Republic of Korea

[4] These authors contributed equally: Hakhyeon Song, Carlos A. Fernández, Hyeonuk Choi

Experimental Section

Materials

Carbon black (Vulcan XC-72R), carbon paper (Sigracet 39BB, and AvCarb MGL 190), anion exchange ionomer (Sustainion XA-9 Ionomer), anion exchange membrane (Sustainion X37-50 Grade RT) and bipolar membrane (Fumasep FBM) were purchased from Fuel Cell store. $KHCO_3$ (ACS reagent, 99.7%), K_2CO_3 (ACS reagent, >99%), KOH (ACS reagent, >85%), potassium nitrate (KNO_3, ACS reagent, ≥99.0%), sodium nitrite ($NaNO_2$, ACS reagent, ≥97.0%), potassium sulfate (K_2SO_4, ACS Reagent, ≥99.0%, Sigma-Aldrich), 2-methylimidazole (2-MeIm, 99%), $Ni(NO_3)_2 \cdot 6H_2O$ (99.999%), cation exchange ionomer (Nafion 117 containing solution, 5%) were obtained from Sigma-Aldrich. Isoprophyl alcohol (IPA) was purchased from VWR. Ethanol (94.0%) was purchased from OCI Company. Sulfuric acid (H_2SO_4, Extra Pure, 95) was obtained from Daejung Chemicals & Metals. All purchased materials were used as received without any additional purification steps.

Synthesis of Ni-based single-atom catalyst (Ni-SAC)

The synthesis of the Ni-based single-atom catalyst (Ni-SAC) involved the following steps. First, 1 g of carbon black (CB), 2.7 g of 2-methylimidazole (2-MeIm), and 0.6 g of $Ni(NO_3)_2 \cdot 6H_2O$ were simultaneously dispersed in 500 mL of ethanol and sonicated for 30 minutes using a sonicator to ensure thorough mixing of the precursors. The solvent in the solution was then removed using a rotary evaporator, resulting in a well-mixed precursor powder. The dried powder was subsequently ground using a mortar and pestle. Next, the ground powder was calcinated at 800 °C with a temperature increase rate of 5 °C per minute in a tube furnace under an Ar flow condition. After the calcination step,

the obtained powder was once again ground using a mortar and pestle to ensure the formation of a homogeneous catalyst.

Fabrication of the Ni-SAC electrodes

The Ni-SAC electrodes for a gas-diffusion electrode (GDE) system were prepared by spray-coating the prepared electrocatalyst ink on the microporous layer sided of hydrophobic carbon paper (Sigracet 39BB). For the electrocatalyst ink preparation, 20 mg of Ni-SAC powder were dispersed in a mixture of 20 mL of ethanol and 125 μL of Nafion 117 solution (5wt%, Sigma-Aldrich). The mixed-ink was sonicated for an hour to make homogenous solution. The well-mixed ink was spray-coated onto carbon paper on a hot plate at 150 ^{o}C until the loading mass per unit area reached to 0.8 mg cm^{-2}.

The Ni-SAC electrodes with different loadings of 1, 2, and 3 mg cm^{-2} for bicarbonate electrolysis were fabricated through a spray-coating method. The catalyst ink, originating from the synthesized Ni-SAC powder (50 mg), combined with a 5% Nafion containing solution (132 μL), mixed with IPA (20 mL). The catalyst ink was ultrasonicated for at least 1 hour. Before spray-coating, a piece of hydrophilic carbon paper (AvCarb MGL 190) was preheated at 110 ^{o}C for an hour to remove any moisture. The prepared catalyst ink was then spray-coated on the carbon paper using an airbrush until the desired catalyst load was achieved (1, 2, and 3 mg cm^{-2}). The catalyst loading was determined by comparing the weight of the electrodes before and after spray-coating process.

Materials characterizations

Scanning electron microscopy (SEM) was performed using Magellan400 (FEI company), and Hitachi SU8230. SEM-energy dispersive spectroscopy (EDS) mapping was performed using Oxford EDS detector (accelerating voltage: 15 kV). Aberration-corrected high-angle annular dark-field scanning electron microscopy (HAADF-STEM) and energy dispersive X-ray spectroscopy (EDS) imaging were conducted using an FEI Titan Cubed G2 60–300 instrument operated at an acceleration voltage of 300 kV. X-ray diffraction (XRD) patterns were collected using a SmartLab (RIGAKU) with a Cu K-alpha-1 incident beam. Inductively coupled plasma mass spectrometer (ICP-MS) was carried out using an iCAP RQ (Thermofisher Scientific). X-ray absorption fine structure (XAFS) spectra of the electrocatalysts were performed using R-XAS with a 2.8 kW power source (RIGAKU). The acquired extended X-ray Absorption Fine. Structure (EXAFS) data was Fourier-transformed and analyzed using the Athena program for accurate interpretation. X-ray photoelectron spectroscopy (XPS) analysis was obtained using a multipurpose XPS instrument (Sigma Probe, Thermo VG Scientific) equipped with an Al K-alpha X-ray source.

Cyclic voltammetry (CV) was conducted within a potential window of ± 40 mV, centered around the open circuit potential (OCP). The measurements were performed at varying scan rates, 50, 75, 100, 150, and 200 mV sec^{-1}, in a 1 M KOH solution to calculate electrochemically active surface area (ECSA) of the Ni-SAC electrodes with different catalyst loadings. For these experiments, a saturated calomel electrode (SCE) containing saturated KCl served as the reference electrode. Additionally, the roughness factor (R_f) was computed by taking the ratio of the double layer capacitance of the electrodes to that of the carbon paper.

$$R_f = \frac{Double\ layer\ capacitance\ of\ electrodes}{Double\ layer\ capacitance\ of\ carbon\ paper}$$

Electrochemical measurements under acid condition in the GDE system

A lab-made gas-fed flow cell was used for all electrochemical measurement. The flow cell was composed of anode and cathode chambers separated by ion-exchange membrane. The prepared Ni-SAC/GDE and commercial iridium oxide electrode (IrO_2/carbon paper, Dioxide Materials) were used as a working and counter electrode, respectively. The 2 cm^2 of both the electrodes was exposed to the electrolyte. Ag/AgCl (saturated KCl, RE-1B, EC-Frontier) electrode and Nafion™ membrane (NRE-212, Alfa Aesar) was used as reference electrode and ion-exchange membrane, respectively. For electrochemical measurement, catholyte was circulated with a peristatic pump (MU-D01, Major Science) from a 50 ml electrolyte reservoir at a flow rate of 10 ml min^{-1}. However, the anolyte was not circulated in the anode compartment (7 ml), which has an opening for generated O_2 gas to escape. Electrolyte with pH 2 and 1 M K^+ was prepared using K_2SO_4 and H_2SO_4.[1] In all electrochemical measurements, chronoamperometry was carried out for 20 min under CO_2 flow rate of 20 sccm, controlled by a mass flow controller (VIC-D210, MFC Korea). A pre-reduction step was conducted at -10 mA cm^{-2} for 10 min before electrochemical test. During electrochemical CO_2 reduction reaction, the solution resistance was measured by the electrochemical impedance spectroscopy at each measurement for ohmic drop (iR) compensation. The ohmic drop was manually compensated with 100%. The applied potentials (vs. Ag/AgCl, $E_{Ag/AgCl}$) of the working electrode were converted to the reversible hydrogen electrode scale (E_{RHE}) using the following equation:

$$\boldsymbol{E_{RHE}\,(V) = E_{Ag/AgCl}\,(V) + 0.059 * pH\,(V) + 0.197\,(V)}$$

Bicarbonate electrolysis measurements

A direct conversion of bicarbonate solution was achieved using a gapless membrane electrode assembly (MEA, Scribner) system with a BPM. The BPM-MEA setup featured a Ni-SAC spray-coated carbon paper (either hydrophilic or hydrophobic) with a geometric area of 5 cm^2 serving as the cathode. This was complemented by BPM, interdigitated flow plates, and a Ni foam anode. The catholyte, 1, 2, or 3 M $KHCO_3$, was circulated through the interdigitated flow plate at a rate of 65 mL min^{-1} using a Masterflex L/S peristaltic pump. Additionally, N_2 gas (99.999% purity, sourced from airgas) was introduced at a flow rate of 200 sccm into the catholyte's headspace via a mass flow controller (MFC, Alicat Scientific). This served as a carrier gas, channeling the generated CO_2, CO, and H_2 gases to a gas chromatograph (GC, SRI Instruments, SRI 8610C). On the anode side, 200 mL of 1 M KOH was circulated at 130 mL min^{-1}. For systems equipped with HCO_3^- regeneration, CO_2 gas (99.999% purity, airgas) was continuously introduced into a 3 M $KHCO_3$ solution at a flow rate of 200 sccm. For the impurity impact experiments, KNO_3, $NaNO_2$, and K_2SO_4 salts were added to the 3 M $KHCO_3$ solution to achieve concentrations of 500 ppm for NO_3^-, NO_2^-, and SO_4^{2-}, individually or in a combined mixture.

Chronopotentiometry (CP) measurements were carried out using either a potentiostat (Gamry instruments, Interface 1000E) and power supply (Maryway Power Solution). Gas products, including CO, H_2, and CO_2, were analyzed over a 30 min duration across various current densities (ranging from -25 to -450 mA cm^{-2}) using GC. The quantification of gases such as N_2, H_2, CO_2, and CO was facilitated by a thermal conductivity detector (TCD) and a flame ionization detector (FID) within the GC. Calibration for each gas was performed at concentrations of 0.5 and 1%.

CO_2 gas electrolysis measurements

CO_2 gas electrolysis was conducted based on the zero-gap membrane electrode assembly (MEA, Dioxide Materials) system. The MEA system is composed of serpentine-type flow channeled cathode and anode substrates separated by AEM. The prepared Ni-SAC spray-coated carbon paper (Sigracet 39BB, 5 cm^2) and Ni foam (5 cm^2) was used as the cathode and anode electrode, respectively. The anolyte, 0.1 M $KHCO_3$, was circulated through the serpentine flow channel at a rate of 20 mL min^{-1} using a peristaltic pump (Masterflex). Additionally, humidified CO_2 gas was fed at a flow rate of 100 sccm into the inlet of the cathode chamber via a mass flow controller (MFC KOREA). The outlet of the cathode chamber was connected directly to GC (6500GC System, YOUNG IN Chromass) equipped with a TCD and an FID for product analysis.

CP measurements were carried out using a potentiostat (BioLogic, VMP3B-10). Gas products, including CO and H_2, and unreacted CO_2 of CP test for 30 min were analyzed from -25 to -300 mA cm^{-2} of total current density using GC equipment.

Nitrogen based products measurements

To measure ammonia, a 5 μl of post-electrolysis solution was diluted with DI water to a total volume of 15 ml. The calibration curve was prepared using the same dilution process, with the addition of 15, 30, and 60 ppm of NH_4^+ (NH_4Cl) to the electrolyte (3 M $KHCO_3$). The ammonia concentration was measured using a Dionex Aquion ion chromatograph (IC, Thermo Fisher Scientific) equipped with a cation-exchange column (CS 12 A). All polyvials and filter caps were thoroughly rinsed with DI water before use to eliminate any potential ammonia contamination. For the mobile phase, a 20 mM methanesulfonic acid

(MSA) eluent was employed, flowing at 0.25 mL min^{-1} through the column. The calibration curves for ammonia and corresponding IC spectra are presented in **Fig. S20, ESI†**.

Calculations of performance metrics

The Faradaic efficiencies of H_2 and CO were calculated by the following equation:

$$FE = \frac{z \times n \times F}{Q}$$

where z is the number of electrons (2 for H_2 and CO) used for formation; n is the number of moles of the CO_2RR products in GC; F is Faradaic constant (96,484 C mol^{-1}); Q is the amount of charge transferred.

The energy efficiency for the CO was calculated as following equation:

$$Energy\ Efficiency\ (\%) = \frac{1.23 + (-E_{CO})}{E_{cell}} \times FE_{CO}$$

where E_{CO} is the thermodynamic energy of CO_2RR to CO (-0.109 V vs. RHE); E_{cell} is the applied cell voltage.

For bicarbonate electrolysis, the CO_2 utilization efficiency was calculated using the following equation:

$$CO_2\ utilization\ efficiency\ (\%) = \frac{moles\ of\ CO_2\ consumed}{moles\ of\ CO_2\ consumed\ +\ moles\ of\ CO_2\ unreacted} \times 100$$

where the moles of CO_2 unreacted were measured based on the detected CO_2 in the GC.

For CO_2 gas electrolysis, the CO_2 utilization efficiency was calculated using the following equation:

$$CO_2\ utilization\ efficiency\ (\%) = \frac{moles\ of\ CO_2\ consumed\ for\ CO_2RR \times 100}{moles\ of\ CO_2\ consumed\ for\ CO_2RR\ and\ carbonates}$$

where the moles of consumed CO_2 consumed for CO_2RR is the moles of CO produced; moles of CO_2 consumed for CO_2RR and carbonate is the differences in moles between inlet and outlet CO_2.

Direct Air Capture System Sizing

The direct air capture (DAC) system is based on pilot tests and modeling done by carbon engineering.[2] The DAC system is sized to capture 0.98 Mt-CO_2 yr^{-1}. The DAC facility is powered partially by electricity input and partially by natural gas input. As such, it produces 1.27 Mt-CO_2 yr^{-1}. The additional 0.29 Mt-CO_2 yr^{-1} come from natural gas combustion in the slacker.

Table S1. Energy requirement for each component in a direct air capture facility.[2]

Parameter	Value	Units
Air Contactor Fluid Pumping Energy	21	kWh t-CO_2^{-1}
Air Contactor Fan Energy	61	kWh t-CO_2^{-1}
Pellet Reactor Fluid Pumping Energy	27	kWh t-CO_2^{-1}
Calciner Energy Consumption	1,125	kWh t-CO_2^{-1}
Slacker Power Production	77	kWh t-CO_2^{-1}
ASU Power Usage	238	kWh t-CO_2^{-1}
Compressor Power Usage	132	kWh t-CO_2^{-1}

The base-power consumption for a DAC system delivering CO_2 at 15 MPa is 5.25 GJ of natural gas and 366 kWh of electricity. However, we have made some modifications to the DAC system in order to integrate with an AEM electrolyzer. The unreacted CO_2 that is lost to carbonate formation is re-introduced to the pellet reactor and recovered as CO_2. As such, for the same production capacity of CO_2, an air contactor that is 22% of the size of the one modeled in the standalone DAC system. The size and energy consumption of the air contactor were scaled down to 22% of its original size.

Additionally, the outlet CO_2 is not compressed to 15 MPa. As such there is no need for a compressor and the power usage for this unit is eliminated. The estimated power consumption for the DAC system coupled with an AEM electrolyzer was recalculated to be 170 kWh tonCO_2^{-1} of electricity and 5.25 GJ tonCO_2^{-1} of natural gas.

For a BPM system operating from bicarbonate, the DAC system only consists of an air contactor. As such, the energy consumption for this system is 82 kWh t-CO_2^{-1} of electricity and no natural gas is needed. These values are modified by the stoichiometry of CO_2:CO and the difference in molar mass between these species. Additionally, in the case of the AEM system, for every mole of CO_2 produced by the DAC, 0.4 moles of CO are produced by the AEM electrolyzer. As such, the values are adjusted by this factor.

Table 2. Direct air capture energy consumption for integrated system with gas-phase AEM and carbonate BPM electrolysis.[2]

Table S2. Direct air capture energy consumption for integrated system with gas-phase AEM and carbonate BPM electrolysis.[2]

System	Direct Air Capture Power Consumption
DAC + AEM	6,395 kWh t-CO^{-1}
DAC + BPM	129 kWh t-CO^{-1}

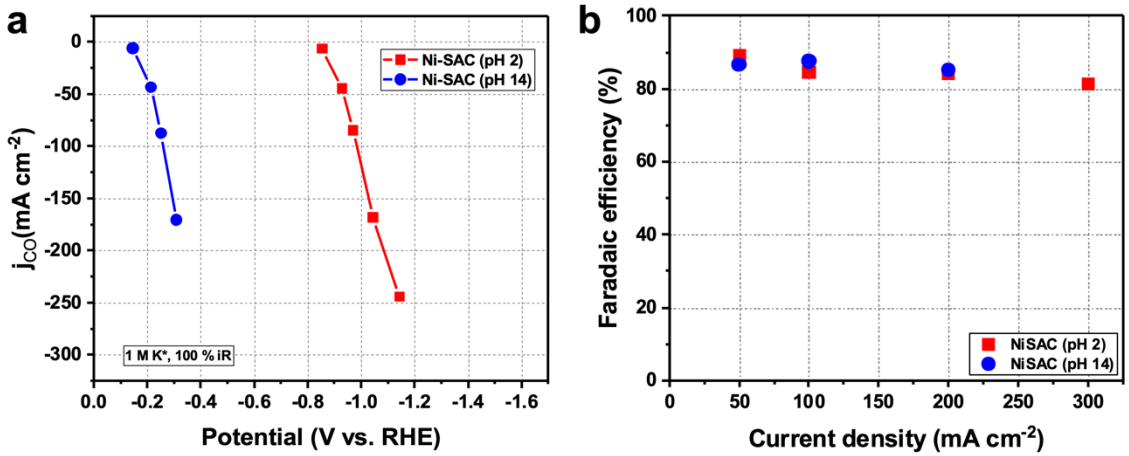

Fig. S1. (a) Partial current densities and (b) Faradaic efficiencies for CO in Ni-single atom catalyst (Ni-SAC) electrodes within a GDE system. Electrolytes: pH 2 (0.01 M H_2SO_4 + 0.5 M K_2SO_4) and pH 14 (1 M KOH). Total potassium concentration: 1 M. The potentials in (a) were calculated with 100% IR compensation after chronopotentiometry.

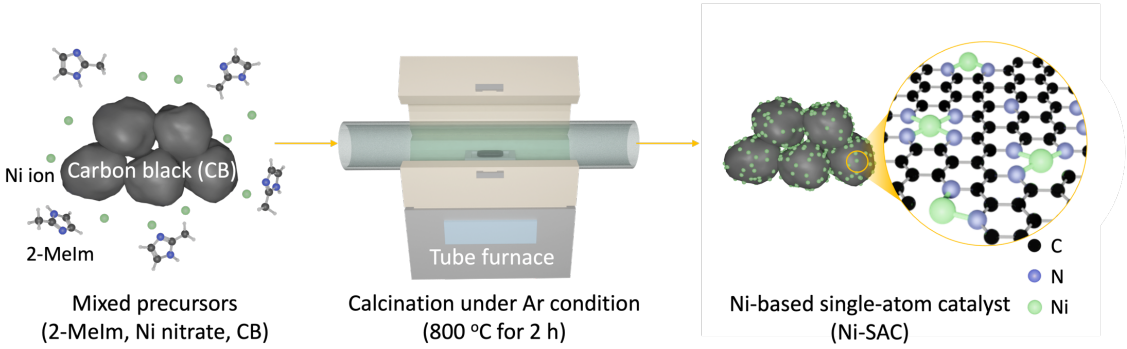

Fig. S2. Schematic representation of the synthesis method for Ni-SAC. Further details on the synthesis procedure can be found in the methods section.

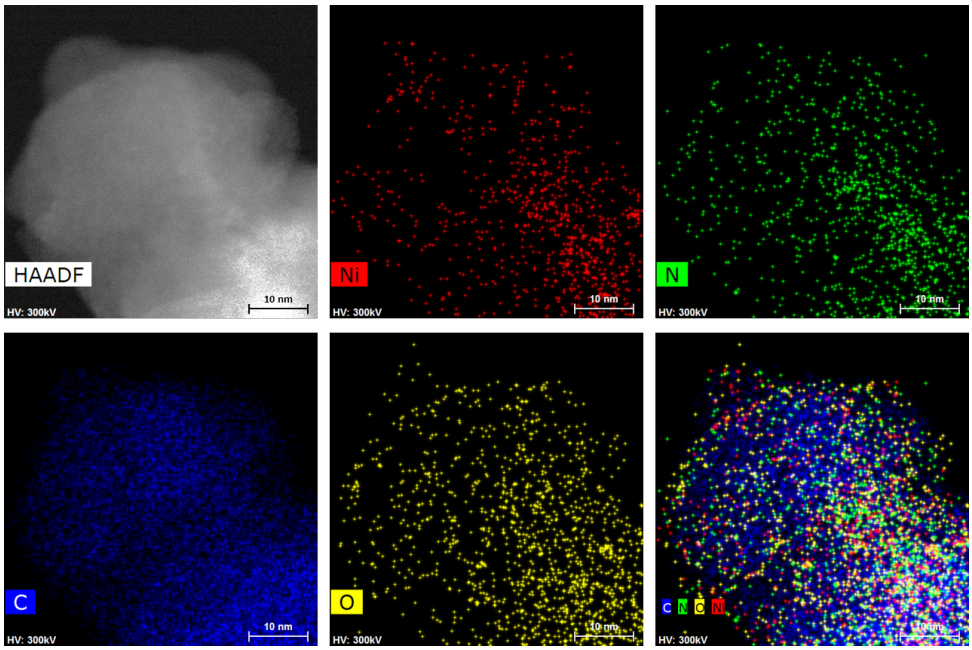

Fig. S3. Scanning transmission electron microscopy-energy-dispersive X-ray spectroscopy (STEM-EDS) mapping of Ni-SAC.

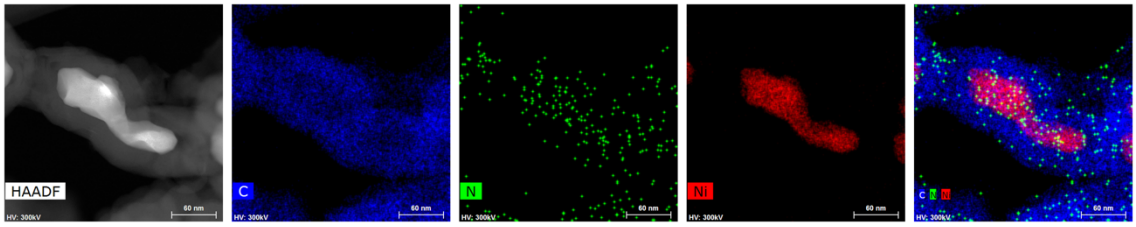

Fig. S4. STEM-EDS mapping of carbon shell covered Ni nanoparticles in Ni-SAC.

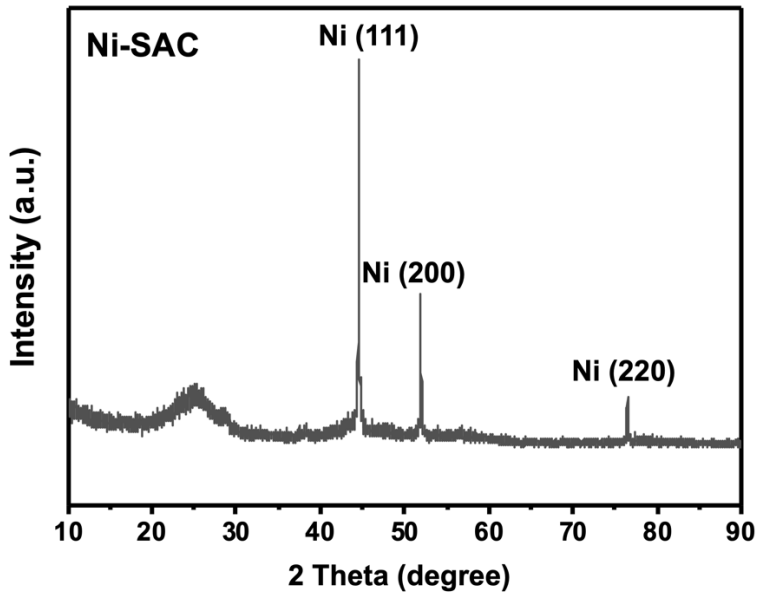

Fig. S5. X-ray diffraction (XRD) of Ni-SAC.

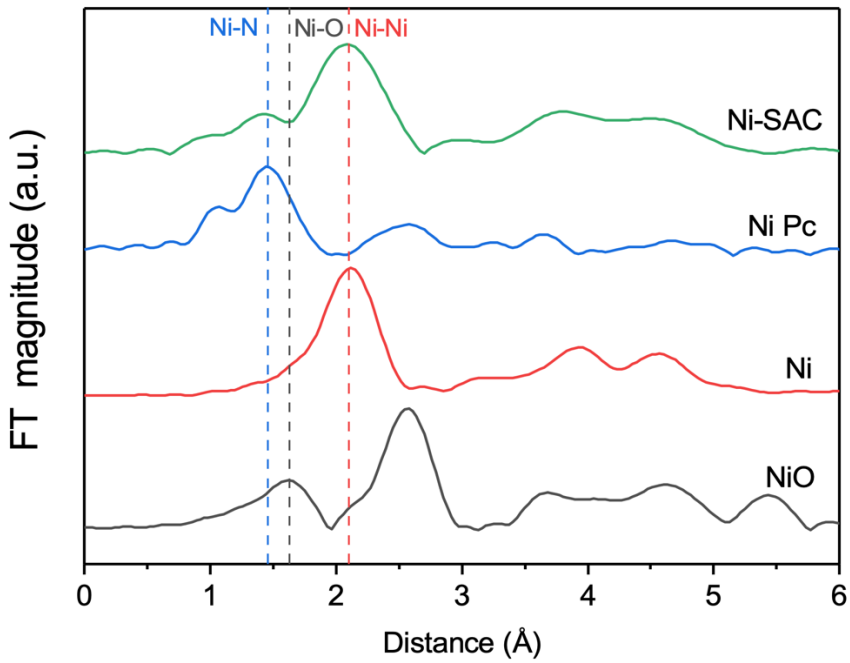

Fig. S6. Fourier-transform of the extended X-ray absorption fine structure (EXAFS) spectrum of metallic Ni, NiO, Ni phthalocyanine (Ni Pc), and Ni-SAC. Ni Pc consists of Ni-N bonding.

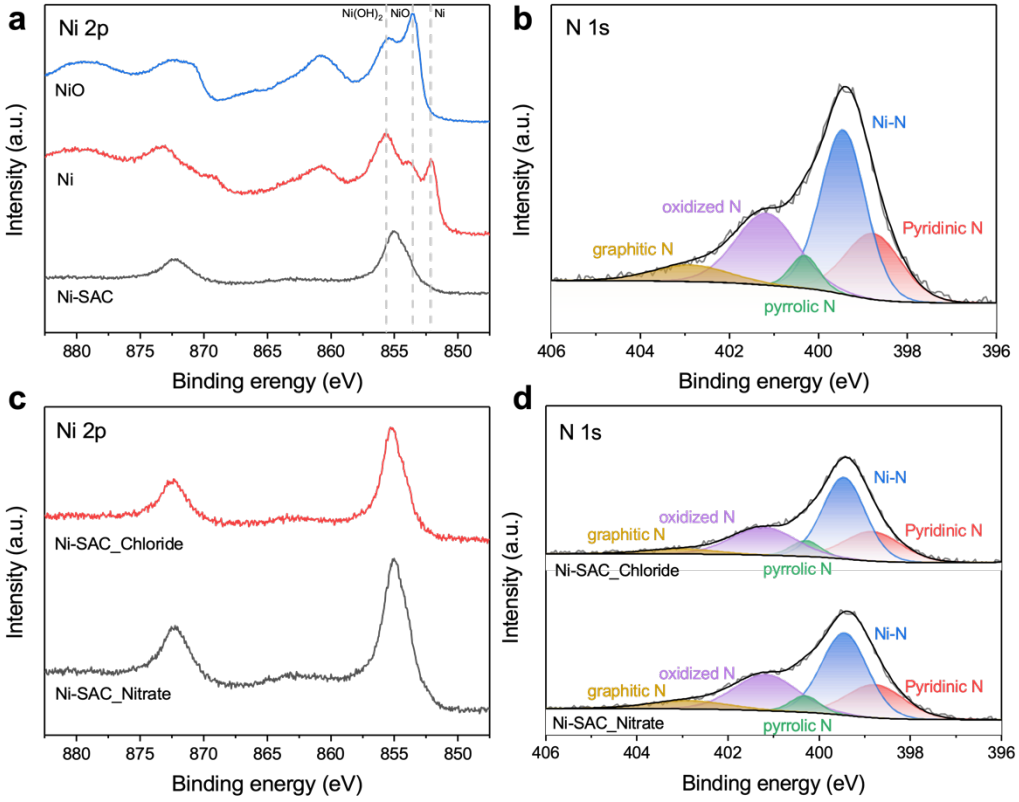

Fig. S7. X-ray photoelectron spectroscopy (XPS) spectrum. (a) Ni 2p of Ni, NiO, and Ni-SAC. (b) N 1s of Ni-SAC. (c) Ni 2p spectrum and (d) N 1s spectrum of Ni-SAC derived from either Ni nitrate or Ni chloride precursors by XPS analysis.

Table S3. Element distribution of Ni-SAC by XPS, ICP-MS, and EDS.

Element	XPS (at%)	XPS (wt%)	ICP (wt%)	EDS (wt%)*
C	84.91	77.09	-	93.81
O	3.84	4.64	-	1.81
N	9.37	9.92	-	2.39
Ni	1.88	8.34	6.32	1.99

* EDS analysis conducted on specific area where Ni NPs are not existed in Ni-SAC.

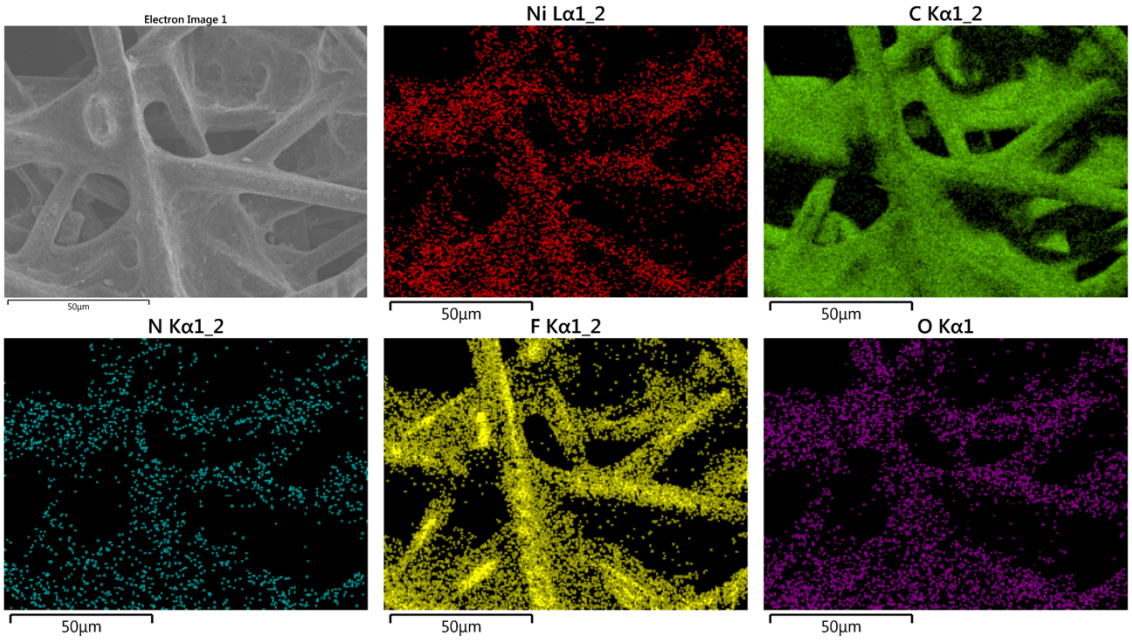

Fig. S8. Scanning electron microscopy-EDS (SEM-EDS) mapping of a Ni-SAC electrode. Each element results from the Ni-SAC, anion exchange ionomer, and carbon paper.

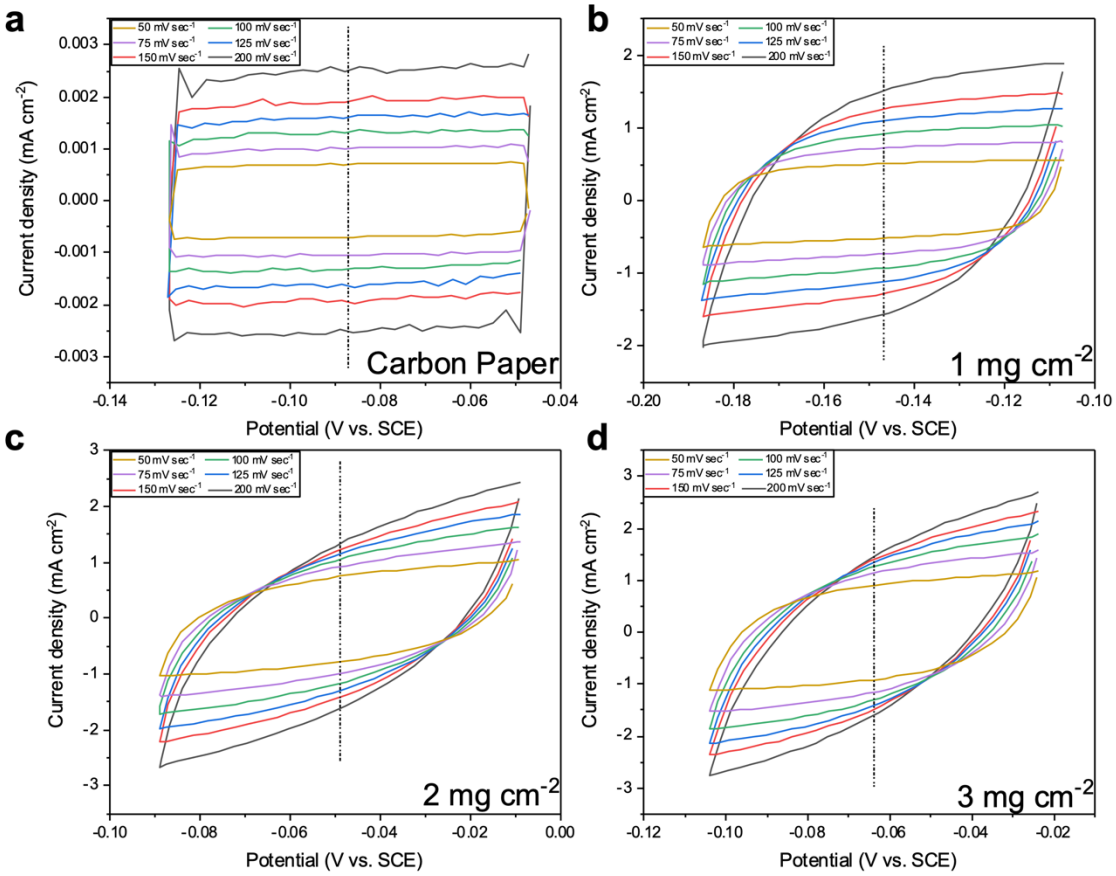

Fig. S9. Cyclic voltammetry (CV) of carbon paper, Ni-SAC electrodes with loadings of (b) 1, (c) 2, and (d) 3 mg cm^{-2}. Measurements taken ±40 mV from open circuit voltage (OCV) at scan rates of 50, 75, 100, 125, 150, and 200 mV sec^{-1}.

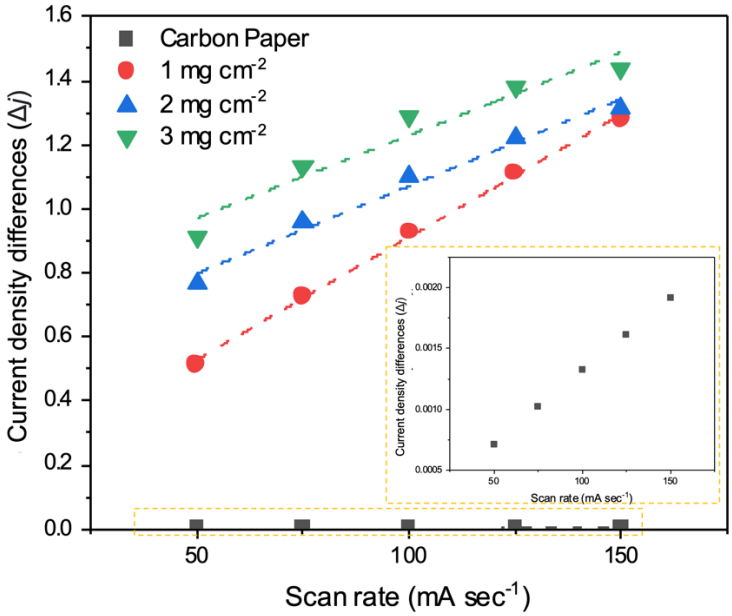

Fig. S10. Electrochemical double layer capacitance of carbon paper, Ni-SAC electrodes at loadings of 1, 2, and 3 mg cm^{-2}. The inset shows a magnified view of the carbon paper.

Table S4. Double layer capacitance and roughness factor of carbon paper and Ni-SAC electrodes with loadings of 1, 2, and 3 mg cm^{-2}.

	Double Layer Capacitance ($\mu F\ cm^{-2}$)	**Roughness Factor**
Carbon Paper	12	1
1 mg cm^{-2}	7,650	~637
2 mg cm^{-2}	5,440	~453
3 mg cm^{-2}	5,170	~430

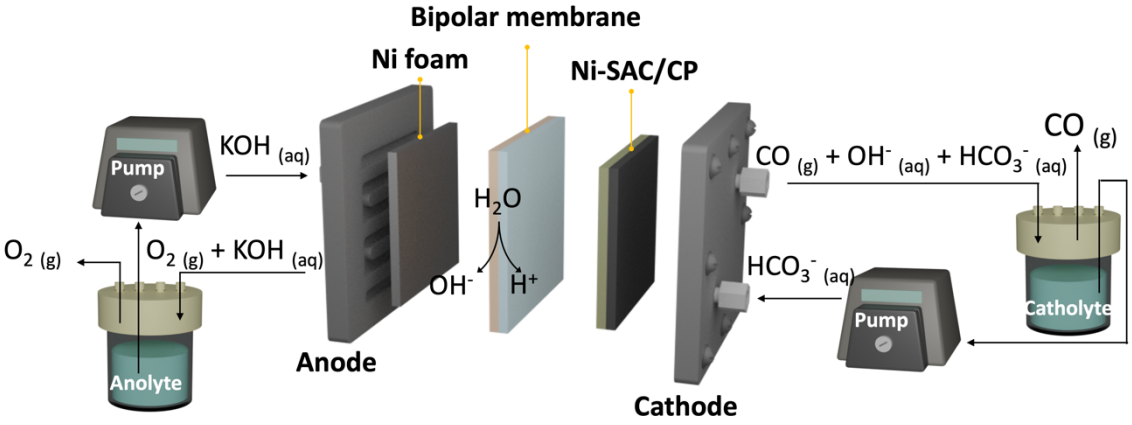

Fig. S11. Schematic representation of electrolysis with a Ni-SAC electrode in conjunction with a bipolar membrane-membrane electrode assembly (BPM-MEA) for bicarbonate conversion.

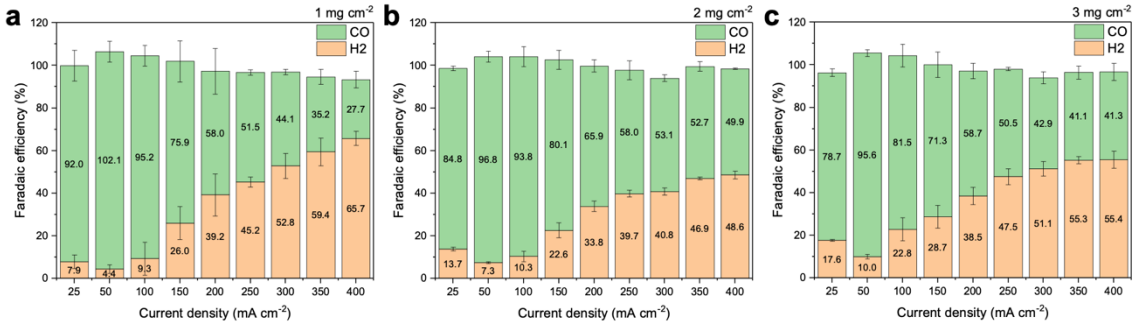

Fig. S12. Faradaic efficiencies for H_2 and CO production using Ni-SAC electrodes at loadings of (a) 1, (b) 2, and (c) 3 mg cm^{-2} over a current density range of -25 to -400 mA cm^{-2}. The duration of electrolysis was 30 minutes. Error bars represent the standard deviation from three separate measurements.

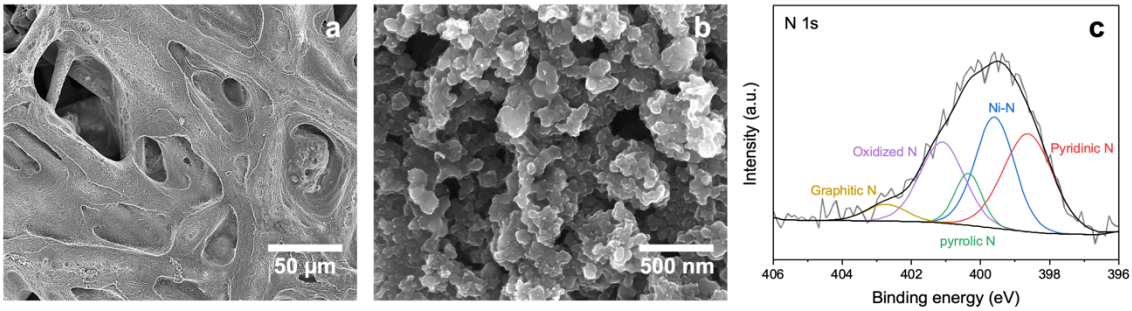

Fig. S13. Post-electrolysis material characterization of a Ni-SAC electrode after 30 min operation. (a) and (b) present morphology by SEM. (c) is N 1s spectrum by XPS.

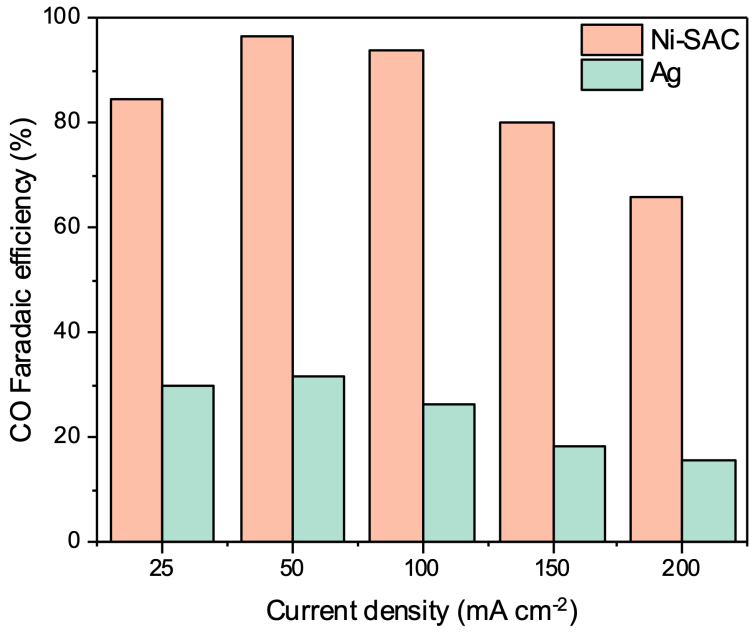

Fig. S14. Comparison of CO Faradaic efficiencies between Ni-SAC and commercial Ag electrodes during bicarbonate electrolysis (3 M $KHCO_3$) over a current density range of -25 to -200 mA cm^{-2}. The catalyst loading for both electrodes is set at 2 mg cm^{-2}.

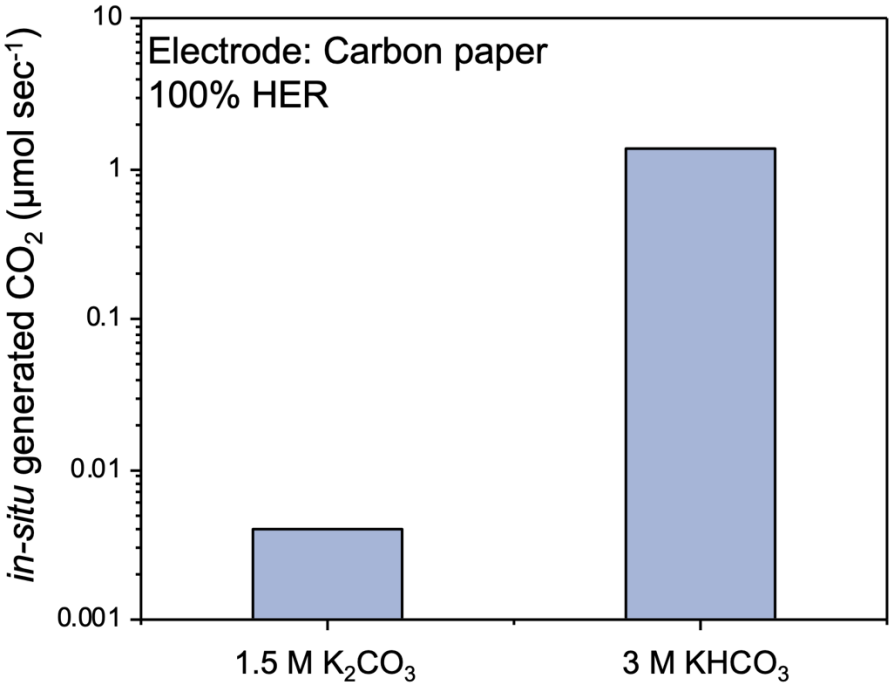

Fig. S15. Comparison of in-situ generated CO_2 between 1.5 M K_2CO_3 and 3 M $KHCO_3$. The in-situ generated CO_2 was quantified from the outlet stream using gas chromatography (GC). The measurement was carried out using carbon paper without a catalyst in a BPM-MEA system.

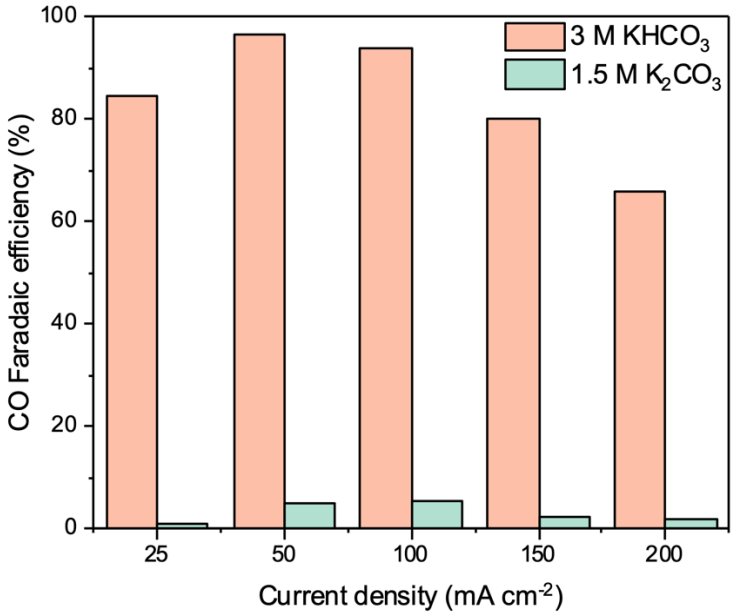

Fig. S16. Comparative analysis of CO production performance in 1.5 M K_2CO_3 and 3 M $KHCO_3$ electrolytes during bicarbonate or carbonate electrolysis using Ni-SAC electrodes.

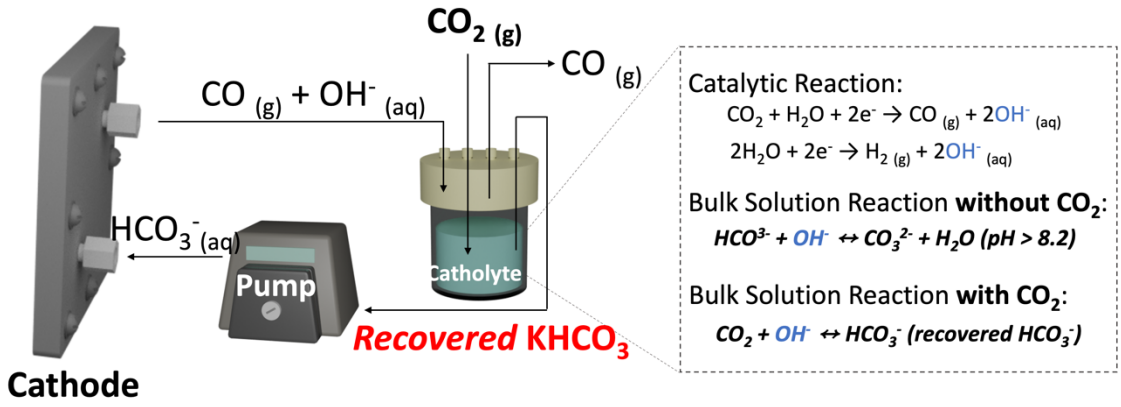

Fig. S17. Schematic of bicarbonate electrolysis with integrated carbon capture (BE-ICC) process. The bicarbonate concentration is replenished through the introduction of CO_2.

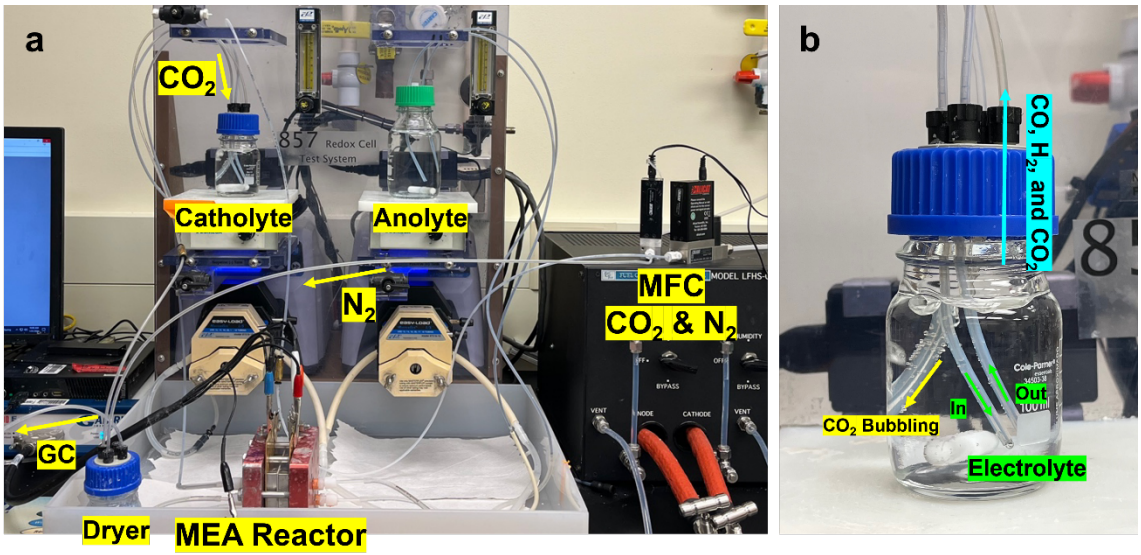

Fig. S18. Photographic depiction of the BE-ICC system. (a) shows the complete BE-ICC setup, capturing the MEA reactor, gas lines for CO_2 and N_2, and the circulation of anolyte and catholyte solutions. Mass flow controllers (MFC) regulate the CO_2 and N_2 gases input. CO_2 is flowed in the catholyte and N_2 is sent through a dryer to deliver produced gases to the gas chromatography (GC) for analysis. (b) Zooms in on the catholyte area where CO_2 gas is bubbled through the electrolyte, ensuring continuous saturation, with the catholyte being recirculated. Generated CO and H_2, in conjunction with CO_2, are transported to the dryer and subsequently to the GC.

Table S5. Comparison of catalytic activity towards CO for bicarbonate or carbonate electrolysis.

Catalyst	*Electrolyte*	*Reactor*	$\lvert j_{total} \rvert$ *(mA cm^{-2})*	FE_{CO} *(%)*	$\lvert j_{CO} \rvert$ *(mA cm^{-2})*	*Cell voltage (V)*	*Ref.*
Ni-SAC	3 M $KHCO_3$	BPM-MEA (BE-ICC)[a]	100	97	97	-3.26	This work
			200	94	188	-3.7	
			300	77	230	-4.3	
			400	63	253	-4.9	
			500	53	263	-5.6	
		BPM-MEA (Semi-batch)[b]	100	94	94	-3.2	
Ag/GDL	3 M $KHCO_3$	BPM-MEA (Semi-batch)[b]	25	81	20.25	-	5
			100	37	37	-	
Free-standing porous Ag	3 M $KHCO_3$	BPM-MEA (Semi-batch)[b]	100	59	59	-3.6	6
Ag foam	3 M $KHCO_3$	HOR|CEM|HCO_3^-[c]	500 (3.5 atm)[c]	44	220	-2.2	7
			500 (1 atm)	15	75	-2.2	
Electrodeposited Ag	3 M $KHCO_3$	BPM-MEA (Semi-batch)[b]	100	68	68	~-3.6	8
Ag	1 M K_2CO_3	BPM-MEA (Semi-batch)[b]	100	28	28	-	9
Ag/CDL[d]	Carbonate from 2 M KOH with	CEM-MEA	200	46	92	~3.7	10

	purging
	CO_2

[a] (Bi)carbonate electrolysis with integrated carbon capture in BPM-MEA
[b] (Bi)carbonate electrolysis without CO_2 flow in BPM-MEA
[c] Pressurized electrolysis with the hydrogen oxidation reaction (HOR) in CEM-MEA
[d] CDL: CO_2 diffusion layer

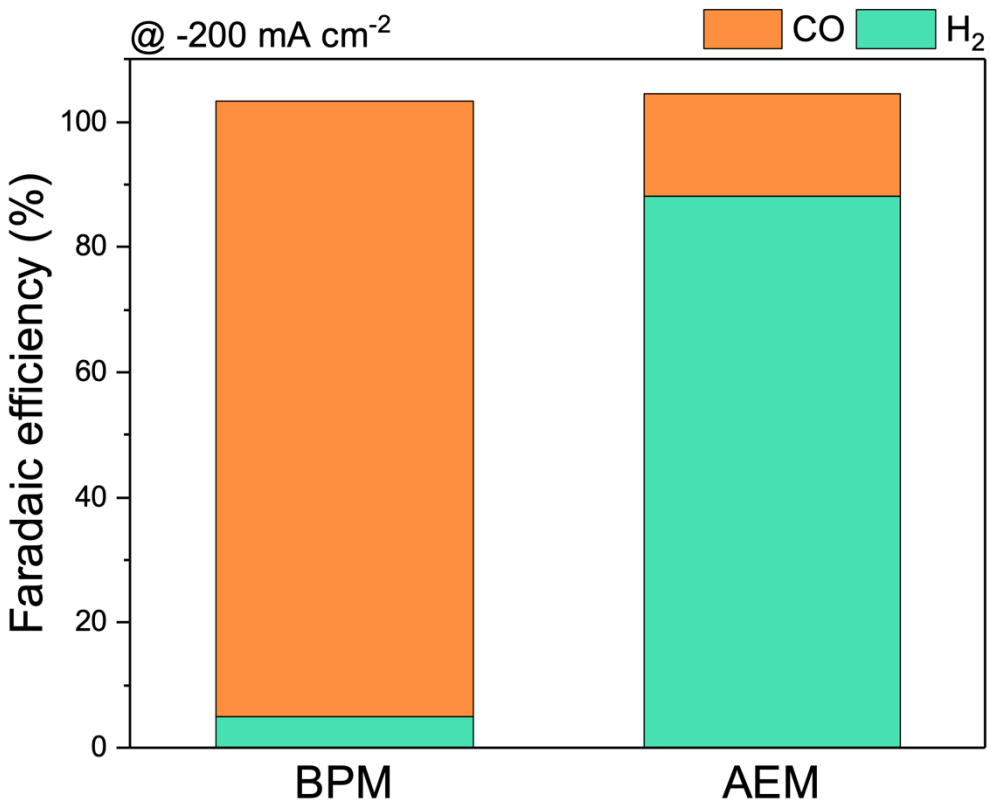

Fig. S19. Comparison of CO performances between BPM-MEA and AEM-MEA systems for bicarbonate electrolysis (3 M $KHCO_3$) at -200 mA cm^{-2}.

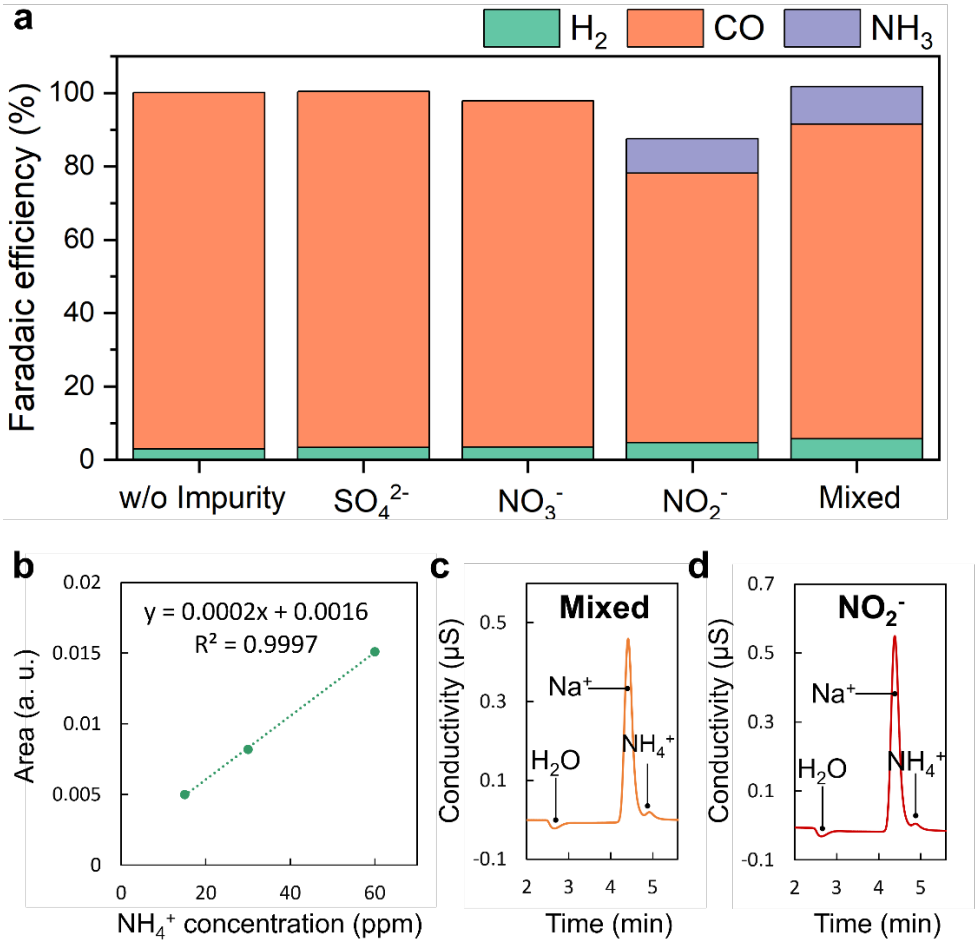

Fig. S20. (a) Product distribution in the BE-ICC system with different impurities under -100 mA cm^{-2}. Impurities were present at a concentration of 500 ppm, with 'mixed' referring to a combination of SO_4^{2-}, NO_3^-, and NO_2^-. (b) calibration curve of ammonia measurement using ionic chromatography (IC) in a 3 M $KHCO_3$ solution. IC spectra showing ammonia peak in solutions with (c) mixed impurities and (d) added NO_2^- in 3 M $KHCO_3$.

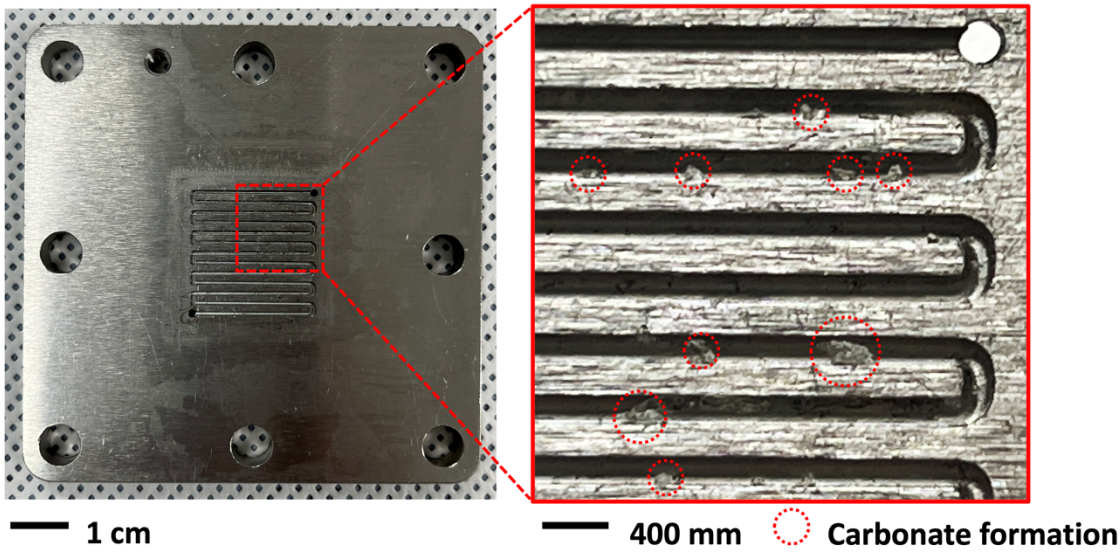

Fig. S21. The formation of carbonate particles in a cathodic flow plate after electrolysis using an AEM-MEA system.

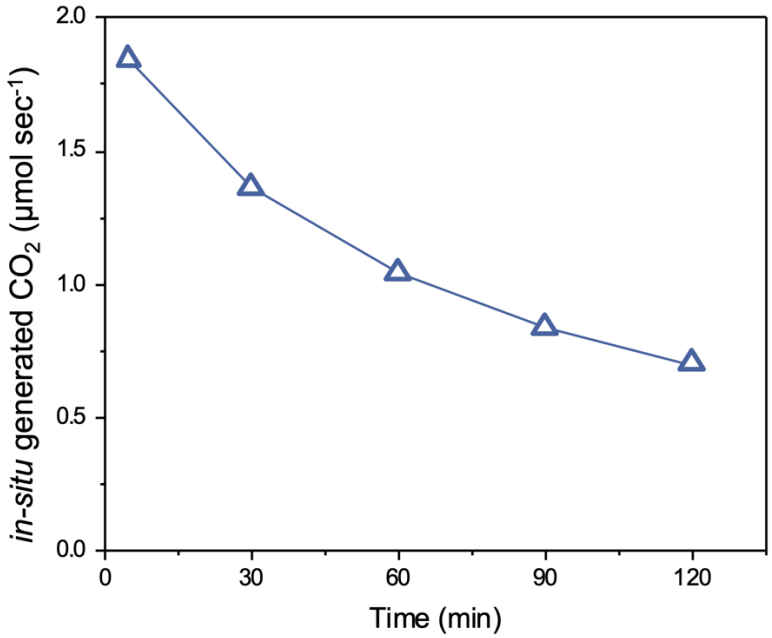

Fig. S22. Change in in-situ generated CO_2 with electrolysis time.

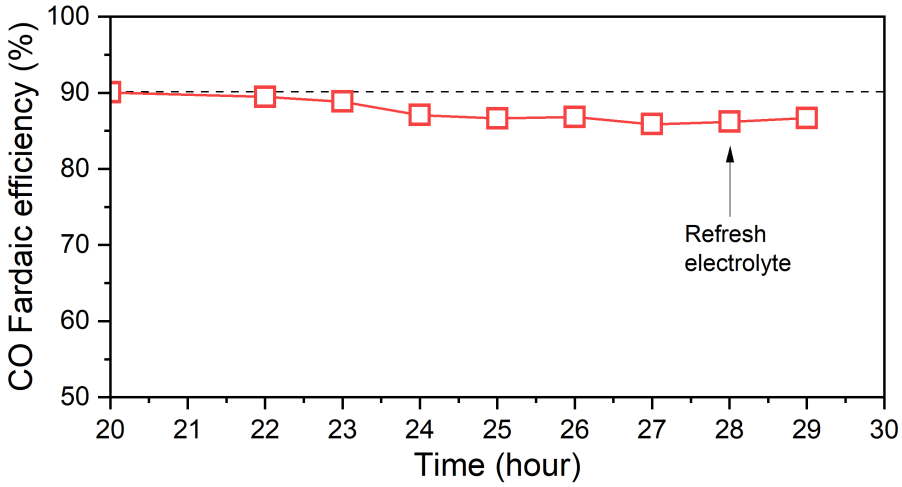

Fig. S23. CO FE over time for the Ni-SAC electrode in the BE-ICC system. The graph illustrates stability beyond 20 hours, with a noted introduction of fresh electrolyte after 28 hours.

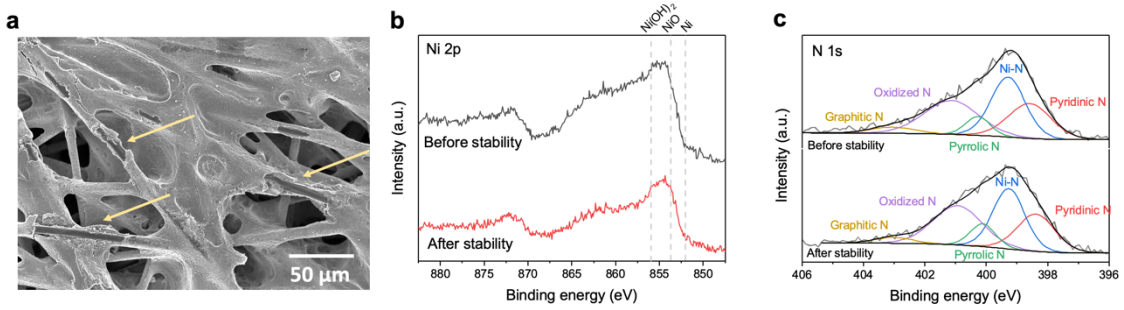

Fig. S24. Material characterization of a Ni-SAC electrode after long-term electrolysis within the BE-ICC system. (a) SEM image of the Ni-SAC electrode, with yellow arrows indicating areas where Ni-SAC partially detached post-electrolysis. XPS spectra of the Ni-SAC electrode showing (b) Ni 2p and (c) N 1s peaks.

References

1. J. Kim, T. H. Ha, J. Kim, G. H. Jeong, S. O. Kim, W. Chung, K. Roh, J. H. Lee and J. Oh, *Appl. Catal. B-Environ.*, 2023, **339**, 123160.
2. D. W. Keith, G. Holmes, D. St. Angelo and K. Heidel, *Joule*, 2018, **2**, 1573-1594.
3. A. Badgett, M. Ruth, A. Crow, G. Grim, Y. Chen, L. Hu, L. Tao, W. Smith, K. C. Neyerlin and R. Cortright, *J. Clean Prod.*, 2022, **351**, 131564.
4. N. Susarla, R. Haghpanah, I. A. Karimi, S. Farooq, A. Rajendran, L. S. C. Tan and J. S. T. Lim, *Chem. Eng. Res. Des.*, 2015, **102**, 354-367.
5. T. Li, E. W. Lees, M. Goldman, D. A. Salvatore, D. M. Weekes and C. P. Berlinguette, *Joule*, 2019, **3**, 1487-1497.
6. Z. Zhang, E. W. Lees, F. Habibzadeh, D. A. Salvatore, S. Ren, G. L. Simpson, D. G. Wheeler, A. Liu and C. P. Berlinguette, *Energy Environ. Sci.*, 2022, **15**, 705-713.
7. Z. Zhang, E. W. Lees, S. Ren, B. A. W. Mowbray, A. Huang and C. P. Berlinguette, *ACS Central Sci.*, 2022, **8**, 749-755.
8. Y. Kim, E. W. Lees and C. P. Berlinguette, *ACS Energy Lett.*, 2022, **7**, 2382-2387.
9. Y. C. Li, G. Lee, T. Yuan, Y. Wang, D.-H. Nam, Z. Wang, F. P. García de Arquer, Y. Lum, C.-T. Dinh, O. Voznyy and E. H. Sargent, *ACS Energy Lett.*, 2019, **4**, 1427-1431.
10. Y. C. Xiao, C. M. Gabardo, S. Liu, G. Lee, Y. Zhao, C. P. O'Brien, R. K. Miao, Y. Xu, J. P. Edwards, M. Fan, J. E. Huang, J. Li, P. Papangelakis, T. Alkayyali, A. Sedighian Rasouli, J. Zhang, E. H. Sargent and D. Sinton, *EES Catal.*, 2023, **1**, 54-61.